Wave Breaking Energy in Coastal Region

Ray-Qing Lin[1] and Lihwa Lin[2]

[1]Dept. of Seakeeping, David Taylor Model Basin, NSWCCD

[2] U.S. Army Engineer Research and Development Center

1. INTERODUCTION

Huang (2006) suggested that wave breaking in the coastal region is a major energy source for the ocean circulation based on the observational data. Because the area of a coastal region is generally 5% or less of the ocean, the energy loss from wave breaking in the coastal region must be significantly greater than in the open ocean.

Two major discoveries in the past have supported Huang's suggestion. In 1980, Herterich and Hasselmann indicated that rapid nonlinear wave-wave interactions could occur and increase as water depth decreased based on the Boltzmann integral method. In 1998, Resio and Tracy, also Lin and Perrie, proved the phenomenon using their numerical models (first using Boltzmann method and later using the Hamiltonian variation principle) as presented at the International Base Enhancement Wave Prediction Conference, Vicksburg, Mississippi. Lin and Perrie (1997) further showed that three wave interactions cannot satisfy the resonant condition in shallow water. Instead, four-wave interactions consisting of three local wind waves interacting with one long wave are required for the resonant in shallow water. Based on these two discoveries, higher frequency and smaller wave amplitude waves no longer dominate in the coastal region. The long wave propagating from the ocean to the coastal region can absorb the wave energy from local wind waves and grow faster than in the deep ocean. This fast nonlinear interaction in coastal region will transfer the energy from higher frequency to lower frequency, and allow the wave to grow faster and cause more energy loss to breaking than in the deep ocean.

Finally, according to the mass conservation law, the wave steepness in the coastal region shall be greater than that in the ocean. This increases the amount of wave breaking as the waves approach the coast, making wave breaking more significant in the coastal region than in the open ocean.

In Section 2, a regional coastal wave model (Lin and Huang, 1996a and b; Lin and Perrie, 1997 and 1999; Lin and Kuang, 2003; Lin and Lin, 2004a and b) is described. Section 3 shows examples of numerical simulation of the nonlinear wave energy transfer. Section 4 shows examples of wave spectral deformation based on field data. Section 5 is for summary and conclusions.

2. COASTAL WAVE MODEL

The base equation for coastal wave model is the action conservation (Lin and Huang, 1996a and b):

$$\frac{\partial A}{\partial t}+\frac{\partial[(c_{gx}+u)A]}{\partial x}+\frac{\partial[(c_{gy}+v)A]}{\partial y}+\frac{\partial[c_\theta A]}{\partial \theta}+\frac{\partial[c_\sigma A]}{\partial \sigma}=S_{in}+S_{ds}+S_{nl}, \qquad (1)$$

where A is the action density equal to N/σ, N is the energy density, σ is the intrinsic frequency, t is the time, θ is the propagation angle, C_{gx}, $C_{gy,}$ C_θ, *and* C_σ are group velocities for *x, y,* θ, and σ coordinates, respectively, S_{in} is the wind input function, S_{ds} is the dissipation function (wave breaking, bottom dissipation, etc.), and S_{nl} is the nonlinear wave-wave interaction. The wind input function for wave generation and dissipation function for wave decay were described by Lin and Lin (2004a and b).

The nonlinear wave-wave interaction, which does not change the total energy, can transform the energy distribution with respect to frequencies and propagation directions. As the energy transfers from high to low frequency (indirect cascades), the waves will grow; as the energy transfers from low to high frequency (direct cascades), waves are dissipated. Often the indirect cascades dominate. The nonlinear source function is

$$\frac{\partial A_{(\mathbf{k}_1)}}{\partial \tau} = 4\pi \iiint_{-\infty}^{\infty} T^2_{i,1,2,3}\,\delta(\mathbf{k}_i + \mathbf{k}_1 - \mathbf{k}_2 - \mathbf{k}_3)\cdot\delta(\omega_i + \omega_1 - \omega_2 - \omega_3)\cdot \{A_{(\mathbf{k}_3)}A_{(\mathbf{k}_2)}[A_{(\mathbf{k}_1)} + A_{(\mathbf{k}_i)}] - A_{(\mathbf{k}_1)}A_{(\mathbf{k}_i)}[A_{(\mathbf{k}_3)} + A_{(\mathbf{k}_2)}]\}d\mathbf{k}_1 d\mathbf{k}_2 d\mathbf{k}_3, \tag{2}$$

Equation (2) can be simplified to a quasi-line integration. Being integrated along the resonant orbit (Tracy and Resio, 1982) and using the resonant solutions that have a highly nonlinear distribution, the strong nonlinear solutions are concentrated in a small area and resonant solutions are small in most areas (Lin and Perrie, 1999). Equation (2) thus becomes

$$\frac{\partial A_{(\mathbf{k}_1)}}{\partial \tau} = 4\pi \int_{\mathbf{k}_i-\Delta\mathbf{k}}^{\mathbf{k}_i+\Delta\mathbf{k}} d\mathbf{k}_2 \int_{\theta_i'-\Delta\theta}^{\theta_i'+\Delta\theta} d\theta\,[2\oint ds \left|\frac{\partial OB(\mathbf{s},\mathbf{n})}{\partial \mathbf{n}}\right|^{-1}]\cdot T^2_{i,1,2,3} \{A_{(\mathbf{k}_3)}A_{(\mathbf{k}_2)}[A_{(\mathbf{k}_1)} + A_{(\mathbf{k}_i)}] - A_{(\mathbf{k}_1)}A_{(\mathbf{k}_i)}[A_{(\mathbf{k}_3)} + A_{(\mathbf{k}_2)}]\}d\mathbf{k}_1 d\mathbf{k}_2 d\mathbf{k}_3, \tag{3}$$

where $T_{i,1,2,3}$ is expressed in Appendix A.

3. NUMERICAL SIMULATION RESULTS

Using quasi-line integration, Eq. (3), examples of numerical simulation of the nonlinear wave energy transfer at different wave depths based on JONSWAP and Pierson-Moskowitz (P-M) spectra are shown in Figs 1 and 2, respectively (Lin and Perrie, 1999). These numerical model results clearly show wave-wave interactions increase as water depth decreases. The nonlinear energy transfer is stronger in a wider frequency range for the P-M spectrum than JONSWAP because the initial P-M spectrum contains more energy than JONSWAP in these examples.

4. FIELD OBSERVATIONS

Wave spectral data collected from three Pacific Coast buoys maintained by the Coastal Data Information Program (CDIP) (http://cdip.ucsd.edu) and National Data Buoy Center (NDBC) (http://www.ndbc.noaa.gov) were used to show the nonlinear wave energy transfer. Figure 3 shows the location map for Buoys 46005, 46029, and 46211. Basically, Buoy 46005 collects the deepwater wave data while 46029 and 46211 measure intermediate and shallow water waves. The surface wind is collected at

NDBC Buoys 46005 and 46029. Table 1 presents coordinates, water depth and data collection period for these buoys.

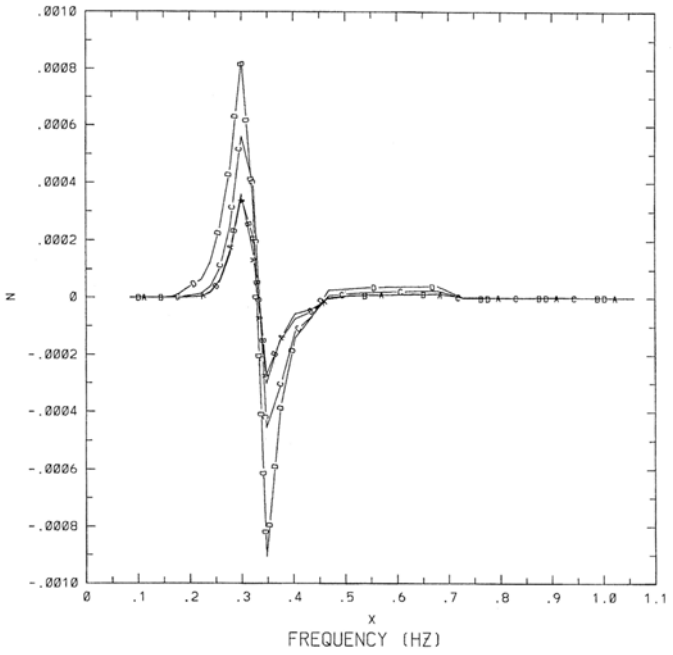

Figure 1. One-dimensional nonlinear transfer rate for JONSWAP spectra: lines A, B, C, and D represent *kh* = 36.3, 1.58, 1.0 and 0.8 (Lin and Perrie, 1999)

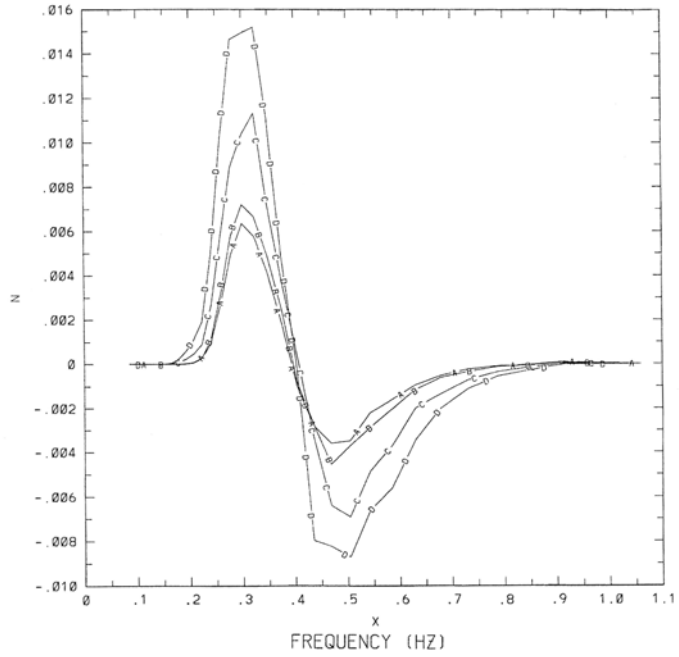

Figure 2. One-dimensional nonlinear transfer rate for P-M spectra: lines A, B, C, and D represent *kh* = 36.3, 1.58, 1.0 and 0.8 (Lin and Perrie, 1999)

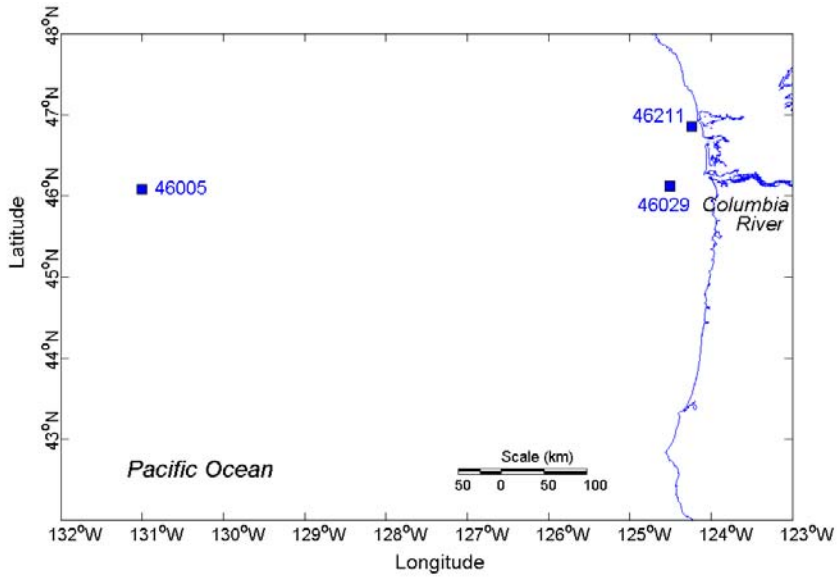

Figure 3. Location Map of Pacific Coast buoys

Table 1 Buoy Station Information			
Station	Coordinates	Depth (m)	Data collection period
NDBC 46005	46^{o} 03' 00" N, 131^{o} 01' 12" W	2853	September 1976 – December 2004
NDBC 46029	46^{o} 07' 00" N, 124^{o} 30' 36" W	128	March 1984 – September 2006
CDIP 46211	46^{o} 51' 24" N, 124^{o} 14' 40" W	39	November 1981 – September 2006

To illustrate the nonlinear wave energy transfer from the data, it is convenient to select the case with small or mild wind condition so that the wind input interference will be minimal. However, the initial wave needs to be large enough that the energy dissipation is relatively small compared to the nonlinear transfer rate. Figure 4 shows time series of measured waves and winds at three buoys for October 1997. Wave energy transfer rates were calculated for one-dimensional frequency spectra collected around 12^{th} and 16^{th} as both wave and wind conditions seem ideal for the illustration of nonlinear wave-wave interactions.

On 12 October 1997, the significant wave height was approximately 2 m and spectral peak period was 9 sec at the three buoys. The dominant wave direction measured at Buoys 46029 and 46211 was approximately from NWW. The wind was moderate at 6 to 7 m/sec from W. Figures 5 through 7 show representative one-dimensional transfer rates estimated at three buoy locations. In these figures, the shallow water wave range is defined as $kh < 0.31416$ and the deepwater range is defined as $kh > 1.571$ (Dean and Dalrymple, 1984). Therefore, the majority of the wave population at Buoy 46005 likely occupies the deepwater range. On the other hand, waves at Buoys 46211 and 46029 are more likely in shallow and intermediate waters, respectively. The deepwater wave spectrum at Buoy 46005 is close to a broad P-M formation. However, measured wave spectra in the intermediate depth (Buoy 46029) and in shallow water (Buoy 46211) have shown multiple peaks (Figs 6 and 7) as a result of nonlinear energy

transfer and wave-bottom interaction. The data show that the spectral peak period is longer in the intermediate depth (Buoy 46029) than in the deep water (Buoy 46005), and the longest period is in the shallow water condition (Buoy 46211). The shape of the nonlinear transfer rate in the frequency domain is similar to the theoretical prediction (Figs 1 and 2). In shallow water (Buoy 46211), because the initial spectrum has multiple peaks, the observed nonlinear transfer rate is seen as the result of combining several single peak spectral energy transfers (Fig 7). The magnitude of nonlinear transfer rate is greater in shallow water than in intermediate and deepwater ranges. This also agrees with the theory (Section 2).

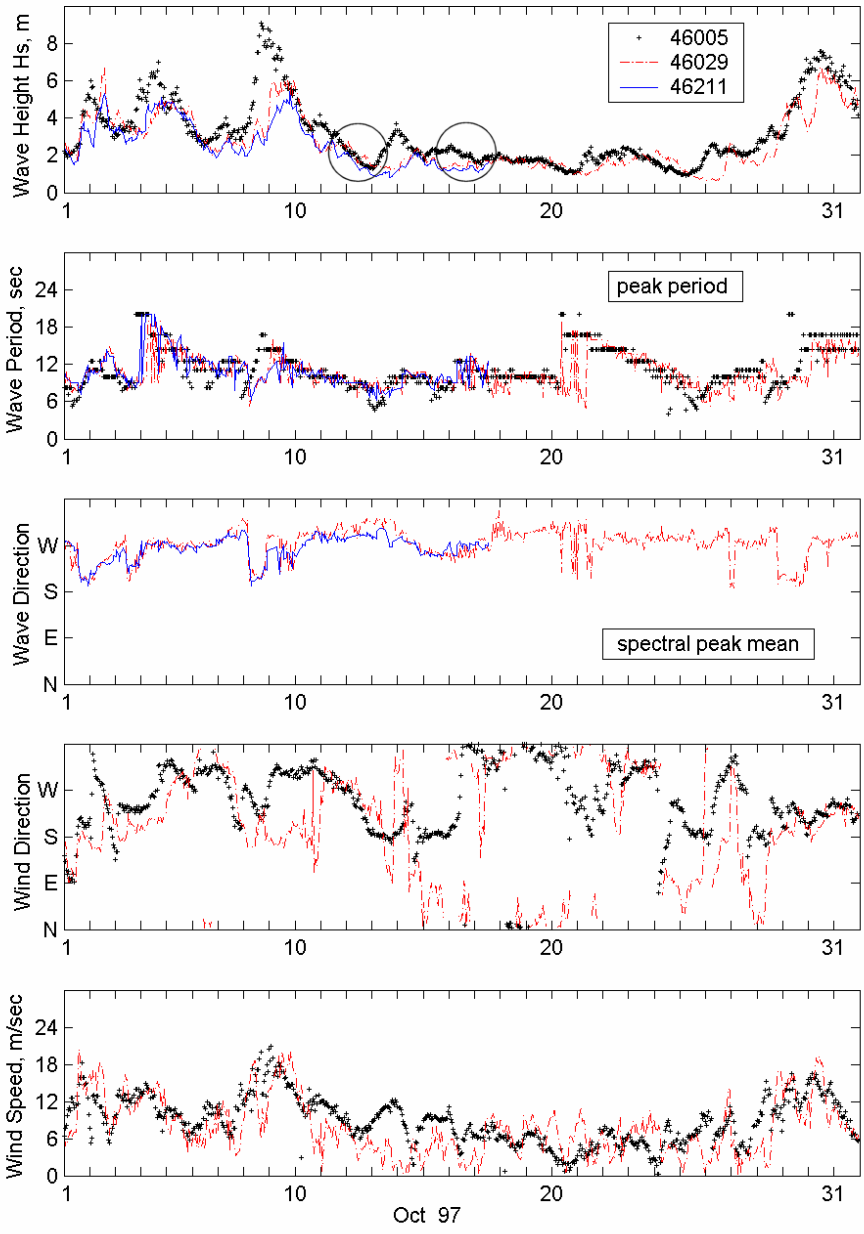

Figure 4. Time series of wave and wind data at Buoys 46005, 46029, and 46211 for October 1997 – two time periods for the illustration of nonlinear energy transfer are shown in circles

On 16 October 1997, the significant wave height was approximately equal to 2 m at the deepwater buoy (46005) and 1.5 m in the intermediate water (46029) and shallow water (46211). The spectral peak period was between 8 and 9 sec at the three buoys. The dominant wave direction measured at Buoys 46029 and 46211 was from W. The surface wind averaged 10 m/sec in the deepwater buoy and 3 m/sec in intermediate and shallow water buoys. The wind direction was from N. Figures 8 to 10 show representative one-dimensional transfer rates estimated at three buoys. The initial deepwater spectrum at Buoy 46005 resembles a broad P-M spectrum. However, wave spectra collected from Buoys 46029 and 46211 in intermediate and shallow waters appear bimodal (Figs 9 and 10) as a result of interaction of two wave systems from different directions in addition to the nonlinear energy transfer. The nonlinear transfer rate in the frequency domain is also similar to the theoretical prediction (Figs 1 and 2). In the shallow and intermediate water depths, because the initial spectra contain multiple peaks, the nonlinear transfer rate becomes more complicated than that in a single peak spectral energy transfer (Fig 10). The magnitude of nonlinear transfer rate is overall greater in shallow and intermediate waters than in the deepwater range.

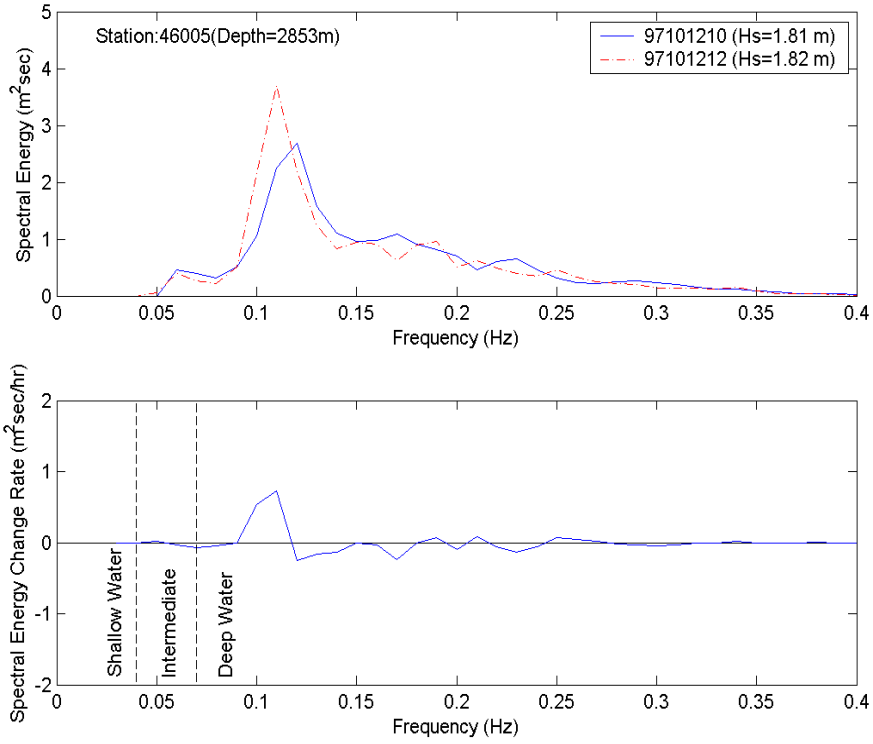

Figure 5. Measured one-dimensional frequency spectra at 10:00 and 12:00 GMT, 12th October 1997 and spectral energy change rate estimation at Buoy 46005

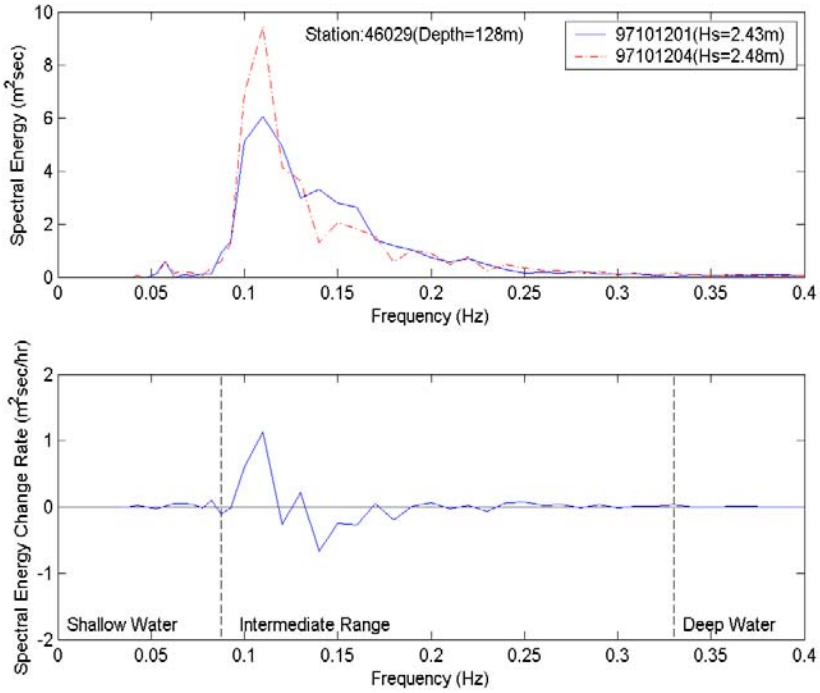

Figure 6. Measured one-dimensional frequency spectra at 01:00 and 04:00 GMT, 12th October 1997 and spectral energy change rate estimation at Buoy 46029

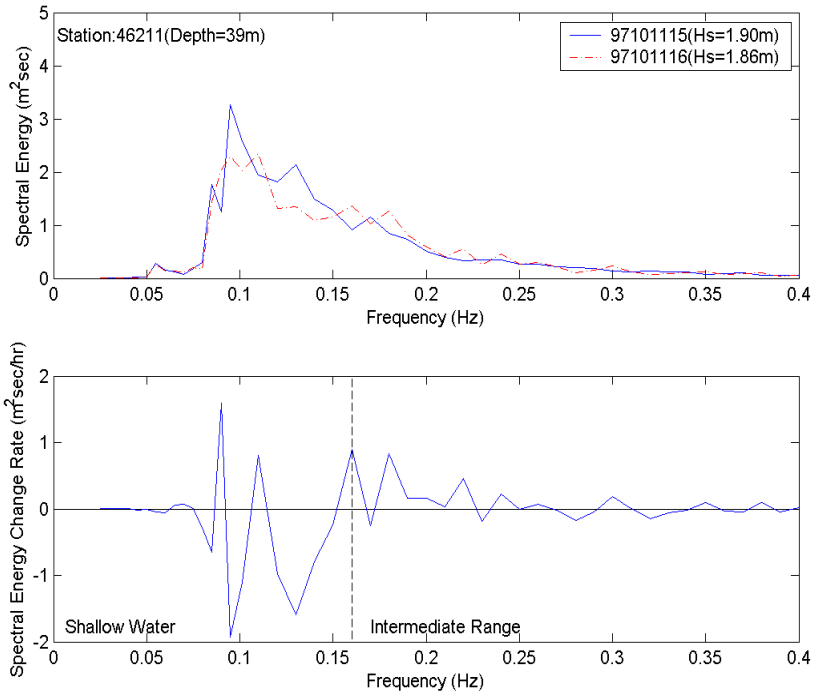

Figure 7. Measured one-dimensional frequency spectra at 15:00 and 16:00 GMT, 11th October 1997 and spectral energy change rate estimation at Buoy 46211

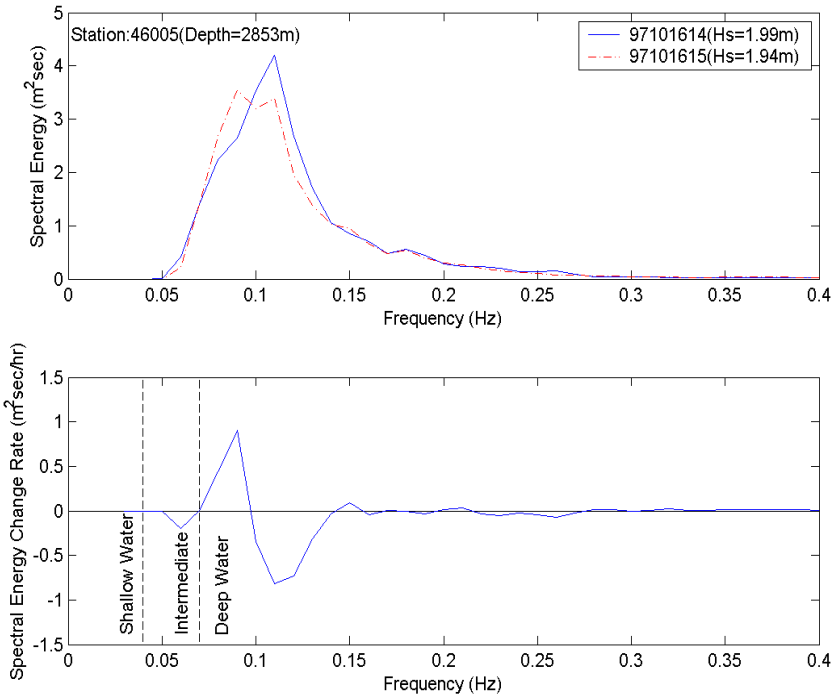

Figure 8. Measured one-dimensional frequency spectra at 14:00 and 15:00 GMT, 16th October 1997 and spectral energy change rate estimation at Buoy 46005

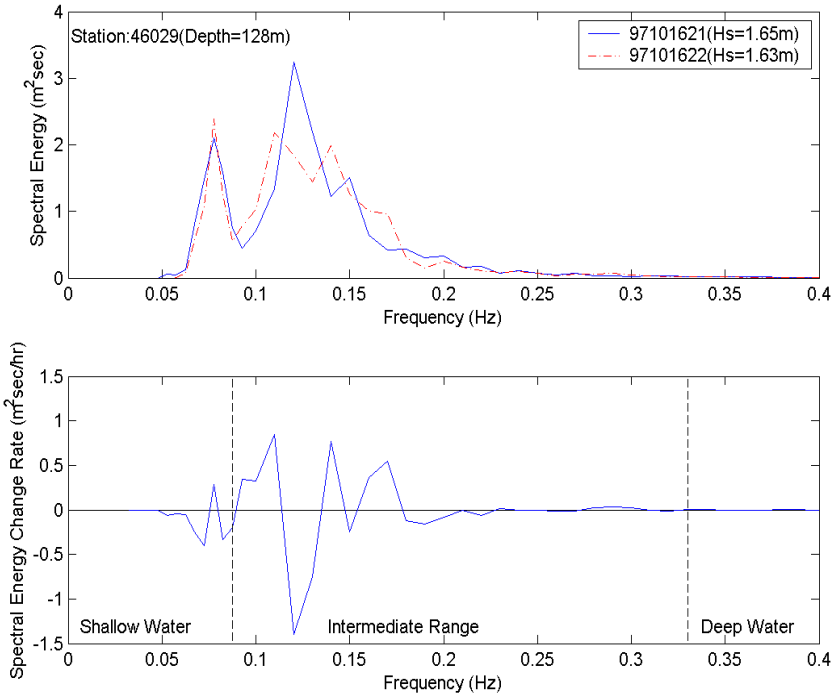

Figure 9. Measured one-dimensional frequency spectra at 21:00 and 22:00 GMT, 16th October 1997 and spectral energy change rate estimation at Buoy 46029

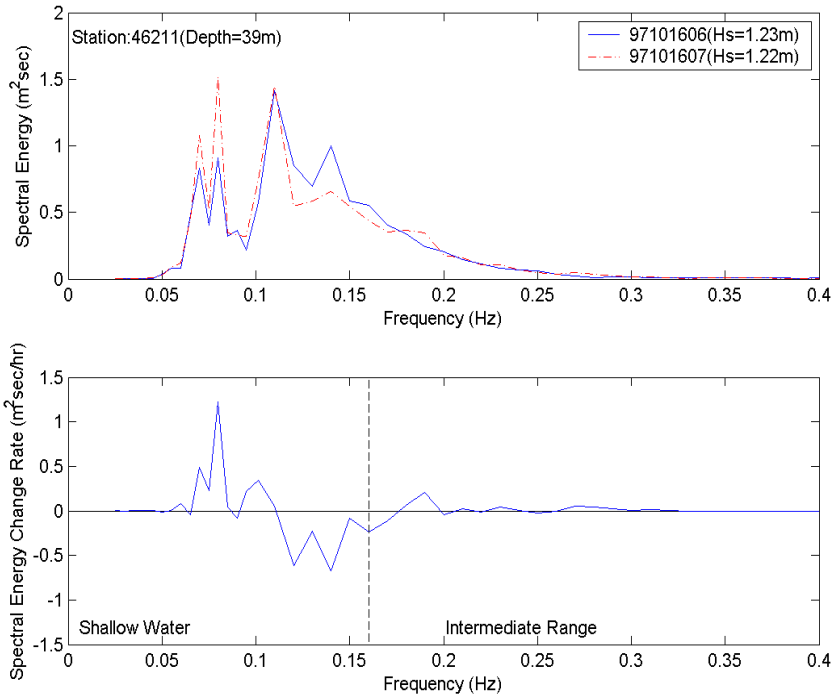

Figure 10. Measured one-dimensional frequency spectra at 06:00 and 07:00 GMT, 16th October 1997 and spectral energy change rate estimation at Buoy 46211

5. SUMMARY AND CONCLUSIONS

Huang (2006) suggested that wave breaking in the coastal region is a major energy source for the ocean circulation based on observational data. Since the coastal regions account for 5% or less of the ocean area, the wave breaking energy in the coastal region shall be much greater than in the open ocean, in addition to relatively larger wave steepness in the shallower water.

The field observational data collected from three Pacific Coast buoys were investigated for the nonlinear energy transfer in different water depth. Wave spectra measured around the 12th and 16th of October 1997 were used to calculate the energy transfer rate in the frequency domain. The shape and relative magnitude of calculated transfer rates were compared for the nonlinearity of wave-wave interactions in deepwater, intermediate, and shallow water ranges. The energy transfer rate calculated in the frequency domain from data appears to agree well with the theory (Figs 1 and 2). Figures 5 through 10 are evidence that nonlinear interactions increase with water deep decrease. The maximum transfer rate from high to low frequency, equal to 1.7 m^2sec/hr, occurred at the shallow water buoy (46211), and the minimum transfer rate from high to low frequency, 0.65 m^2sec/hr, occurred at the deep water buoy (46005).

The effect of stronger nonlinear interaction in the shallow water region is the transfer of more energy from shorter waves into longer waves in the coastal region. These large, longer waves break in the shallow water, and a small fraction of the energy can be reflected back to the ocean, resulting in stronger currents along the coast.

Acknowledgements

The authors would like to thank Mr. Terry Applebee for providing many useful comments and suggestions to this study. We also thank Dr. John Barkyoumb for supporting the numerical modeling project under the Office of Naval Research's In-House Laboratory Independent Research (ILIR) Program at NSWCCD.

References

Dean, R.G. and R.A. Dalrymple. 1984: Water Wave Mechanics for Engineers and Scientists. Prentice-Hall, Inc., Englewood Cliffs, New Jersey.

Herterich, K. and K. Hasselmann, 1980: A Similarity Relation for the Nonlinear Energy Transfer in a Finite Depth Gravity-wave Spectrum, *J. of Fluid Mech*., **97**, 215-224.

Huang, R.-X., 2006: Energy Source of Ocean Circulation, submitted to *J. of Phys. Ocean*.

Lin, L. and R.-Q. Lin, 2004a: Wave Breaking Function, the *8th International Workshop on Wave Hindcasting and Prediction*. North Shore, Oahu, Hawaii. November 14-19.

Lin, R.-Q. and N. Huang, 1996a: The Goddard Coastal Wave Model, Part I: Numerical Method. *J. Physical Oceanography*, **26**, 833-847.

Lin, R.-Q. and N. Huang, 1996b: The Goddard Coastal Wave Model, Part II: Numerical Method. *J. Physical Oceanography*, **26**, 848-862.

Lin, R.-Q. and W. Kuang, 2003: Finite Amplitude Wave-wave Interactions in a Global Statistical Wave Prediction Model. *Recent Res. Devel. Phys Oceanography*, 45-59 ISBN, 45-59.

Lin, R.-Q. and L. Lin, 2004b: Wind Input Function, the *8th International Workshop on Wave Hindcasting and Prediction*. North Shore, Oahu, Hawaii. November 14-19.

Lin, R.-Q. and W. Perrie, 1997: A New Coastal Wave Model, Part III: Nonlinear Wave-wave Interaction, *J. Physical Oceanography*, **27**, 1813-1826.

Lin, R.-Q. and W. Perrie, 1999: Wave-wave Interactions in Finite Depth Water, *J. of Geophysical Research*, **104**, No. C5, 11193-11213.

Resio, Don and Barbara Tracy, 1998: Nonlinear Wave-wave Interaction Source Function in Finite Water. International Base Enhancement Wave Prediction Conference, Vicksburg, Mississippi.

Tracy, B.A. and D.T. Resio, Theory, 1982: Theory and Calculation of the Nonlinear Energy Transfer Between Sea Waves in Deep Water, WIS Rep. 11, 50 pp. U.S. Army Eng. Waterways Exp. Station, Vicksburg, Mississippi.

APPENDIX A

$$
\begin{aligned}
T_{i,1,2,3} = & -V^{(-)}_{(\mathbf{k}_3,\mathbf{k}_3-\mathbf{k}_1,\mathbf{k}_1)} V^{(-)}_{(\mathbf{k}_i,\mathbf{k}_2-\mathbf{k}_i\cdot\mathbf{k}_2)} \{\frac{1}{\omega_{(\mathbf{k}_1-\mathbf{k}_3)}-\omega_{(\mathbf{k}_3)}+\omega_{(\mathbf{k}_1)}}+\frac{1}{\omega_{(\mathbf{k}_2)}-\omega_{(\mathbf{k}_i-\mathbf{k}_2)}+\omega_{(\mathbf{k}_i)}}\} \\
& -V^{(-)}_{(\mathbf{k}_2,\mathbf{k}_i,\mathbf{k}_2-\mathbf{k}_1)} V^{(-)}_{(\mathbf{k}_1,\mathbf{k}_1-\mathbf{k}_3,\mathbf{k}_3)} \{\frac{1}{\omega_{(\mathbf{k}_1-\mathbf{k}_3)}-\omega_{(\mathbf{k}_1)}+\omega_{(\mathbf{k}_3)}}+\frac{1}{\omega_{(\mathbf{k}_i)}-\omega_{(\mathbf{k}_2-\mathbf{k}_i)}+\omega_{(\mathbf{k}_2)}}\} \\
& -V^{(-)}_{(\mathbf{k}_2,\mathbf{k}_2-\mathbf{k}_1,\mathbf{k}_1)} V^{(-)}_{(\mathbf{k}_i,\mathbf{k}_3-\mathbf{k}_i\cdot\mathbf{k}_3)} \{\frac{1}{\omega_{(\mathbf{k}_1-\mathbf{k}_2)}-\omega_{(\mathbf{k}_2)}+\omega_{(\mathbf{k}_1)}}+\frac{1}{\omega_{(\mathbf{k}_3)}-\omega_{(\mathbf{k}_3-\mathbf{k}_i)}+\omega_{(\mathbf{k}_i)}}\} \\
& -V^{(-)}_{(\mathbf{k}_3,\mathbf{k}_i,\mathbf{k}_3-\mathbf{k}_1)} V^{(-)}_{(\mathbf{k}_1,\mathbf{k}_1-\mathbf{k}_2,\mathbf{k}_2)} \{\frac{1}{\omega_{(\mathbf{k}_1-\mathbf{k}_2)}-\omega_{(\mathbf{k}_1)}+\omega_{(\mathbf{k}_2)}}+\frac{1}{\omega_{(\mathbf{k}_i)}-\omega_{(\mathbf{k}_3-\mathbf{k}_i)}+\omega_{(\mathbf{k}_3)}}\} \\
& -V^{(-)}_{(\mathbf{k}_i+\mathbf{k}_1\mathbf{k}_i,\mathbf{k}_1)} V^{(-)}_{(\mathbf{k}_2+\mathbf{k}_3,\mathbf{k}_2,\mathbf{k}_3)} \{\frac{1}{\omega_{(\mathbf{k}_i+\mathbf{k}_1)}-\omega_{(\mathbf{k}_i)}-\omega_{(\mathbf{k}_1)}}+\frac{1}{\omega_{(\mathbf{k}_2+\mathbf{k}_3)}-\omega_{(\mathbf{k}_2)}-\omega_{(\mathbf{k}_3)}}\} \\
& -V^{(+)}_{(-\mathbf{k}_2-\mathbf{k}_3,\mathbf{k}_2,\mathbf{k}_3)} V^{(+)}_{(\mathbf{k}_i,\mathbf{k}_1-\mathbf{k}_i-\mathbf{k}_1)} \{\frac{1}{\omega_{(\mathbf{k}_2+\mathbf{k}_3)}+\omega_{(\mathbf{k}_2)}+\omega_{(\mathbf{k}_3)}}+\frac{1}{\omega_{(\mathbf{k}_i+\mathbf{k}_1)}+\omega_{(\mathbf{k}_i)}+\omega_{(\mathbf{k}_1)}}\}+W_{(\mathbf{k}_i,\mathbf{k}_1,\mathbf{k}_2,\mathbf{k}_3)}.
\end{aligned}
\tag{A1}
$$

$$
\begin{aligned}
V^{(\pm)}_{(\mathbf{k}_i,\mathbf{k}_1,\mathbf{k}_2)} = & \frac{1}{8\pi\sqrt{2}} \{[\mathbf{k}_i\cdot\mathbf{k}_1 \pm k_i k_1 \tanh(k_i h)\tanh(k_1 h)][\frac{\omega_{(k_i)}\omega_{(k_1)} k_2 \tanh k_2 h}{\omega_{(k_2)} k_i k_1 \tanh k_i h \tanh k_1 h}]^{\frac{1}{2}} \\
& +[\mathbf{k}_i\cdot\mathbf{k}_2 \pm k_i k_2 \tanh(k_i h)\tanh(k_2 h)][\frac{\omega_{(k_i)}\omega_{(k_2)} k_1 \tanh k_1 h}{\omega_{(k_1)} k_i k_2 \tanh k_i h \tanh k_2 h}]^{\frac{1}{2}} \\
& [\mathbf{k}_i\cdot\mathbf{k}_2 + k_1 k_2 \tanh(k_1 h)\tanh(k_2 h)][\frac{\omega_{(k_1)}\omega_{(k_2)} k_i \tanh k_i h}{\omega_{(k_i)} k_1 k_2 \tanh k_1 h \tanh k_2 h}]^{\frac{1}{2}},
\end{aligned}
\tag{A2}
$$

and

$$
\begin{aligned}
W_{(\mathbf{k}_i,\mathbf{k}_1,\mathbf{k}_2,\mathbf{k}_3)} = & \overline{\mathrm{W}}_{(\text{-}\mathbf{k}_i,\text{-}\mathbf{k}_1,\mathbf{k}_2,\mathbf{k}_3)} + \overline{\mathrm{W}}_{(\mathbf{k}_2,\mathbf{k}_3,-\mathbf{k}_i,-\mathbf{k}_1)} - \overline{\mathrm{W}}_{(\mathbf{k}_2,\text{-}\mathbf{k}_1,\mathbf{k}_i,\mathbf{k}_3)} - \overline{\mathrm{W}}_{(\text{-}\mathbf{k}_i,\mathbf{k}_2,-\mathbf{k}_1,\mathbf{k}_3)} \\
& - \overline{\mathrm{W}}_{(\text{-}\mathbf{k}_i,\mathbf{k}_3,\mathbf{k}_2,\mathbf{k}_1)} - \overline{\mathrm{W}}_{(\mathbf{k}_3,\text{-}\mathbf{k}_1,\mathbf{k}_2,-\mathbf{k}_i)}
\end{aligned}
\tag{A3}
$$

$$
\begin{aligned}
\vec{W}_{(\mathbf{k}_i,\mathbf{k}_1,\mathbf{k}_2,\mathbf{k}_3)} = & \frac{1}{64\pi}[\frac{\omega_{(k_i)}\omega_{(k_1)}}{\omega_{(k_2)}\omega_{(k_3)}} k_i k_1 k_2 k_3 \tanh(k_i h)\tanh(k_1 h)\tanh(k_2 h)\tanh(k_3 h)]^{\frac{1}{2}} x \\
& [2(\frac{\mathrm{k_i}}{\tanh \mathrm{k_i} h}+\frac{\mathrm{k_1}}{\tanh \mathrm{k_1} h}) - |\mathbf{k}_1+\mathbf{k}_3| \tanh(|\mathbf{k}_1+\mathbf{k}_3| h) - |\mathbf{k}_1+\mathbf{k}_2| \tanh(|\mathbf{k}_1+\mathbf{k}_2| h) \\
& - |\mathbf{k}_i+\mathbf{k}_3| \tanh(|\mathbf{k}_i+\mathbf{k}_3| h) - |\mathbf{k}_i+\mathbf{k}_2| \tanh(|\mathbf{k}_i+\mathbf{k}_2| h)
\end{aligned}
\tag{A4}
$$